Soliton excitations on a continuous-wave background in the modulational instability regime with fourth-order effects

Liang Duan,[1,2] Li-Chen Zhao,[1,2,*] Wen-Hao Xu,[1,2] Chong Liu,[1,2] Zhan-Ying Yang,[1,2,†] and Wen-Li Yang[2,3]

[1]*School of Physics, Northwest University, 710069 Xi'an, China*

[2]*Shaanxi Key Laboratory for Theoretical Physics Frontiers, 710069 Xi'an, China*

[3]*Institute of Modern Physics, Northwest University, 710069 Xian, China*

(Received 27 October 2016; revised manuscript received 7 March 2017; published 19 April 2017)

We study the correspondence between modulational instability and types of fundamental nonlinear excitation in a nonlinear fiber with both third-order and fourth-order effects. Some soliton excitations are obtained in the modulational instability regime which have not been found in nonlinear fibers with second-order effects and third-order effects. Explicit analysis suggests that the existence of solitons is related to the modulation stability circle in the modulation instability regime, and they just exist in the modulational instability regime outside of the modulational stability circle. It should be emphasized that the solitons exist only with two special profiles on a continuous-wave background at a certain frequency. The evolution stability of the solitons is tested numerically by adding some noise to initial states, which indicates that they are robust against perturbations even in the modulation instability regime. Further analysis indicates that solitons in the modulational instability regime are caused by fourth-order effects.

DOI: 10.1103/PhysRevE.95.042212

I. INTRODUCTION

Modulation instability (MI) is a fundamental process associated with the growth of perturbations on a continuous-wave background (CWB) [1]. It can be used to understand the dynamics of nonlinear waves on a CWB, such as the Akhmediev breather [2,3], Peregrine rogue wave [4,5], and Kuznetsov-Ma breather [6,7] and even high-order rogue waves [8–13]. Different MI gain distributions could bring different nonlinear excitation pattern dynamics [14]. We presented rational W-shaped solitons in the modulational stability (MS) regime [15], and autonomous transition dynamics from the MI to the MS regime on critical boundary lines between MI and MS regimes [16]. Recently a few authors have suggested that baseband MI or MI with resonant perturbations could induce rogue-wave excitation as a universal property of different nonlinear models [17–20]. Furthermore, quantitative correspondence relations between nonlinear excitations and MI were clarified based on the dominant perturbation frequency for the simplest nonlinear Schrödinger equation (NLSE) [20]. The correspondence between MI and nonlinear excitations will be very meaningful for controllable excitation [21]. Therefore, it is meaningful and essential to obtain the correspondence relation between MI and nonlinear excitations in other physical cases [22].

High-order effects are usually taken to describe the nonlinear dynamics more precisely for many physical systems. For example, nonlinear susceptibility will produce high-order nonlinear effects like the Kerr dispersion (i.e., self-steepening), the delayed nonlinear response, and even the third-order dispersion for ultrashort pulses whose duration is shorter than 100 fs in a nonlinear fiber. Recently, we obtained correspondence relations between MI and nonlinear excitations for the Sasa-Satsuma [16] and Hirota [23] models, which are the NLSE with some third-order effects. Those results indicate that third-order effects cause great variation in MI properties, which would induce some new nonlinear excitations. We extend the previous studies to consider the NLSE with both third-order and fourth-order effects [see Eq. (1)] and perform a linear stability analysis on a CWB. We find an MS circle in the MI regime (see Fig. 1). This is topologically different from the finite-width MS band for the Sasa-Satsuma model [16] and the MS line for the Hirota equation [23]. We have obtained many nonlinear dynamics in the NLSE with high-order effects. For example, rational W-shaped solitons [14] and multipeak solitons [23] have been reported. It is naturally expected that there should be much more abundant nonlinear excitation dynamics in this case.

In this paper, we study the correspondence relation between MI and fundamental excitations in the NLSE with both third-order and fourth-order effects. These fundamental excitations—including mainly the Akhmediev breather, rogue wave, Kuznetsov-Ma breather, periodic wave, W-shaped soliton train, rational W-shaped soliton, antidark (AD) soliton, and nonrational W-shaped (WS_{nr}) soliton—can be described by an exact solution in a generic form. Especially, AD and WS_{nr} soliton excitations can exist in the MI regime outside the MS circle, in sharp contrast to the correspondence relation for the simplest NLSE [20], Hirota equation [23], and Sasa-Satsuma equation [16]. When the soliton perturbation energy on a CWB tends to 0, the stable perturbations agree with the linear stability analysis results. When the soliton perturbation energy is nonzero, the stable perturbations do not agree with the linear stability analysis results. It should be emphasized that the solitons just exist with two special profiles on a certain-frequency CWB, and the existence of solitons in the MI regime is caused by fourth-order effects. We further test the evolution stability of solitons numerically, which indicates that they are robust against perturbation even in the MI regime.

Our presentation of the above features is structured as follows. In Sec. II, a linear analysis on a CWB is performed and a generic exact solution is given for types of fundamental non-

*zhaolichen3@nwu.edu.cn

†zyyang@nwu.edu.cn

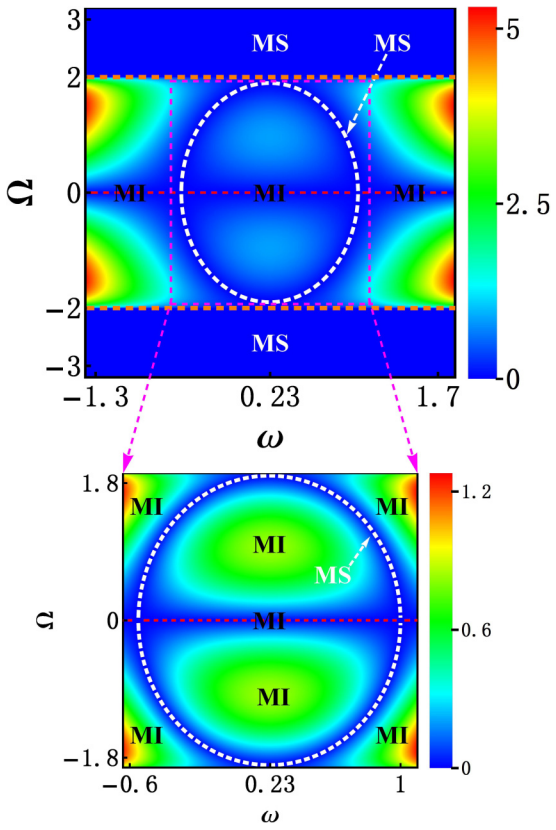

FIG. 1. Modulation instability (MI) gain G distribution on the background frequency ω and perturbation frequency Ω plane. MS, modulation stability. There is an MS circle in the MI band, shown by the dashed white line. The MI gain value is not 0 for the regime outside and inside of the MS circle, shown in the lower frame. Parameters are $A = 1$, $\beta = \frac{1}{6}$, and $\gamma = -\frac{5+\sqrt{15}}{48}$.

linear excitations. The correspondence between MI and these fundamental nonlinear excitations is presented. Especially, AD solitons and WS_{nr} solitons can exist in the MI regime, which is absent for the NLSE, Sasa-Satsuma, and Hirota models. In Sec. III, we discuss the AD soliton and WS_{nr} soliton in the MI regime and test their stability numerically. It is found that solitons just exist with a special profile on a certain-frequency CWB, and the existence of solitons in the MI regime is caused by fourth-order effects. Finally, we summarize the results and present our discussion in Sec. IV.

II. CORRESPONDENCE BETWEEN MODULATIONAL INSTABILITY AND SEVERAL FUNDAMENTAL NONLINEAR EXCITATIONS

Many efforts have been made to study nonlinear excitations in nonlinear fibers with high-order effects, such as the Sasa-Satsuma equation [15,16,24–27] and Hirota equation [28–30]. The Sasa-Satsuma and Hirota equations are NLSEs with third-order effects. Some recent experiments and theoretical studies have suggested that fourth-order effects could play an important role in soliton dynamics in nonlinear fibers [31]. Moreover, fourth-order effects could play an important role in anisotropic Heisenberg ferromagnetic systems [32,33]. We would like to further consider an NLSE with both third-order and fourth-order effects as [34–39]

$$i\psi_z + \tfrac{1}{2}\psi_{tt} + \psi|\psi|^2 + i\beta H[\psi(t,z)] + \gamma P[\psi(t,z)] = 0, \tag{1}$$

where the third-order $H[\psi(t,z)] = \psi_{ttt} + 6|\psi|^2\psi_t$ is the Hirota operator (beginning with the third-order dispersion), and the fourth-order $P[\psi(t,z)] = \psi_{tttt} + 8|\psi|^2\psi_{tt} + 6\psi|\psi|^4 + 4\psi|\psi_t|^2 + 6\psi_t^2\psi^* + 2\psi^2\psi_{tt}^*$ is the Lakshmanan-Porsezian-Daniel operator (beginning with the fourth-order dispersion). Here, z is the propagation variable and t is the transverse variable (time in a moving frame), with the function $|\psi(t,z)|$ being the envelope of the waves.

When $\beta = \gamma = 0$, Eq. (1) reduces to the standard NLSE, which can be used to describe picosecond optical pulse propagation in fibers. When $\gamma = 0$, Eq. (1) becomes the Hirota equation including the third-order dispersion and $|\psi|^2\psi_t$ term, which was derived in [40]. Moreover, the general governing equation for optical pulse propagation in a fiber can be given as [41] $i\psi_z = -\sum_{m=1}^{\infty}\frac{i^m\beta_m}{m!}\frac{\partial^m\psi}{\partial t^m} - \gamma(1 + is\frac{\partial}{\partial t})(\psi\int_0^\infty R(t')|\psi(t-t')|^2dt')$, where the first term on the right-hand side is the linear dispersion, with corresponding coefficients β_m, while the second term describes the nonlinear terms, taking into account their dispersion. Here, s is the self-steepening coefficient, the nonlinear term γ depends on the effective core area, and $R(t)$ includes instantaneous (electronic) and delayed nuclear (Raman) contributions of the nonlinear material response. The integral in the above equation is often approximated by taking the series to first order only, i.e., $|\psi|^2 - \tau_R$, for Raman delay τ_R. However, in reality, we need to consider higher-order terms. Then some higher-order terms of Eq. (1) can be obtained by choosing the higher-order nonlinear response function $R(t)$ [38].

Additionally, Eq. (1) has been obtained in an anisotropic Heisenberg ferromagnet with Dzyaloshinskii-Moriya interaction which is restricted to the z direction [32]. Furthermore, Eq. (1) with $\beta = 0$ also can be used to describe an anisotropic Heisenberg ferromagnet chain without Dzyaloshinskii-Moriya interaction [33]. In this case, $|\psi|^2$ presents the spin deviation between the spin S and its projection in the z-axis direction S^z.

Since MI properties can be used to understand different excitation patterns on a CWB in nonlinear systems [15,16,20,23], we perform the standard linear stability analysis on a generic CWB $\psi_0 = Ae^{i\theta} = A\,e^{i(kz+\omega t)}$ [A, ω, and $k = A^2 - \frac{1}{2}\omega^2 + \beta(\omega^3 - 6A^2\omega) + \gamma(6A^4 - 12A^2\omega^2 + \omega^4)$ represent the amplitude, frequency, and wave number of the background electric field, respectively]. A perturbed nonlinear background can be written as $\psi_p = (A + p)e^{i\theta}$, where $p(t,z)$ is a small perturbation which is given by collecting the Fourier modes as $p = f_+\exp[i(Kz + \Omega t)] + f_-\exp[-i(Kz + \Omega t)]$, where f_+ and f_- are much less than the background amplitude A, and Ω represents the perturbed frequency. Then one can obtain the MI gain, $G = |\mathrm{Im}(K)| = \mathrm{Im}\Omega\sqrt{(\Omega^2 - 4A^2)[1/2 - 3\beta\omega + \gamma(6A^2 - 6\omega^2 - \Omega^2)]^2}$, by linearizing the nonlinear partial equation and solving the eigenvalue problems. Obversely, there is a low-perturbed-frequency MI regime ($|\Omega| < 2A$) in perturbed-frequency Ω and background-frequency ω space.

TABLE I. Types of nonlinear waves in the fourth-order NLS system. Parameters are $\delta = 2\sqrt{b^2 - A^2}$; $\Omega = \pm 2\sqrt{A^2 - b^2}$; $\chi_k = \delta(t + v_k z)$; $\chi_a = \Omega(t + v_a z)$; $\chi_s = \delta(t + v_s z)$; $\chi_p = \Omega(t + v_p z)$; v_k, v_a, v_r, v_s, v_w, and v_p correspond to the v_1 values in the Appendix under corresponding conditions; $\Lambda = \frac{\sqrt{s^2}}{s}$ ($s = b + \sqrt{b^2 - A^2}$, $|b| > A$); and the phase satisfies $\cos\theta_k = \frac{bs}{A\sqrt{s^2}}$, $\sin\theta_k = i\frac{bs - A^2}{A\sqrt{s^2}}$, $\cosh\mu_{\mathrm{AD}} = b/A$, $\sinh\mu_{\mathrm{AD}} = \sqrt{b^2 - A^2}/A$, where $b > 0$. Other parameters are the same as in the Appendix.

Existence condition	Nonlinear wave type	Analytic expression
$b > A, (\omega + \frac{\beta}{4\gamma})^2 - \frac{\delta^2}{6} \neq \alpha$	Kuznetsov-Ma breather	$[1 - \frac{2b[\Lambda\cos(bv_2\delta z - \theta_k) - \cosh(\chi_k)]}{A\cos(bv_2\delta z) - b\cosh(\chi_k)}]Ae^{i\theta}$
$b < A, (\omega + \frac{\beta}{4\gamma})^2 + \frac{\Omega^2}{6} \neq \alpha$	Akhmediev breather	$[-A - \frac{(2A^2 - 2b^2)\cosh(bv_2\Omega z) + i\Omega b\sinh(bv_2\Omega z)}{b\cos(\chi_a) - A\cosh(2bv_2\Omega z)}]e^{i\theta}$
$b = A, (\omega + \frac{\beta}{4\gamma})^2 \neq \alpha$	Rogue wave	$[\frac{4(2iA^2v_2z + 1)}{1 + 4A^2(t + v_r z)^2 + 4A^4v_2^2z^2} - 1]Ae^{i\theta}$
$b > A, (\omega + \frac{\beta}{4\gamma})^2 - \frac{\delta^2}{6} = \alpha$	Nonrational W-shaped soliton	$[\frac{-\delta^2}{2A - 2b\cosh\chi_s} - A]e^{i\theta}$
$b > A, (\omega + \frac{\beta}{4\gamma})^2 - \frac{\delta^2}{6} = \alpha$	Antidark soliton	$[\frac{-\delta^2}{2A + 2b\cosh(\chi_s - \mu_2)} - A]e^{i\theta}$
$b = A, (\omega + \frac{\beta}{4\gamma}) = \alpha, \alpha \geqslant 0$	Rational W-shaped soliton	$[\frac{4}{1 + 4A^2(t + v_w z)^2} - 1]Ae^{i\theta}$
$\frac{A}{2} < b < A, (\omega + \frac{\beta}{4\gamma})^2 + \frac{\Omega^2}{6} = \alpha, \alpha > 0$	W-shaped soliton train	$[\frac{\Omega^2}{2A - 2b\cos\chi_p} - A]e^{i\theta}$
$0 < b \leqslant \frac{A}{2}, (\omega + \frac{\beta}{4\gamma})^2 + \frac{\Omega^2}{6} = \alpha, \alpha > \frac{A^2}{2}$	Periodic wave	$[\frac{\Omega^2}{2A - 2b\cos\chi_p} - A]e^{i\theta}$

Particularly, when $1/2 - 3\beta\omega + \gamma(6A^2 - 6\omega^2 - \Omega^2) = 0$, i.e.,

$$\left(\omega + \frac{\beta}{4\gamma}\right)^2 + \frac{\Omega^2}{6} = \alpha, \tag{2}$$

the MI gain $G = 0$, where $\alpha = \frac{\beta^2}{16\gamma^2} + \frac{1}{12\gamma} + A^2$. When $\alpha > 0$, the MS regime, Eq. (2), describes an ellipse whose center is localized at point $(-\frac{\beta}{4\gamma}, 0)$. Its semimajor axis is equal to $\sqrt{6\alpha}$ and parallel to the Ω coordinate and its semiminor axis is equal to $\sqrt{\alpha}$ in the ω coordinate. When the semimajor axis is less than $2A$ and greater than 0, all parts of the ellipse are located in the MI regime (see Fig. 1). Namely, the MI band ($|\Omega| \leqslant 2A$) contains a special MS regime which satisfies Eq. (2), which brings the MS circle in the MI regime. Nonzero MI gain values exist in areas both outside and inside the circle (see Fig. 1). It should be noted that the MI gain form fails to predict the stability of perturbations on the resonant line ($\Omega = 0$) [20]. For $\Omega = 0$ mode perturbation denoted $\epsilon\tilde{p}$ (where $\epsilon \ll 1$ is a real constant), we can derive the secular solution as $\tilde{p} = 1 + 24iA^2\gamma[\alpha - (\omega + \frac{\beta}{4\gamma})^2]z$, which demonstrates the instability property of the resonant perturbation mode. The perturbations with modes $(\omega + \frac{\beta}{4\gamma})^2 = \alpha$ on the MS circle do not admit rational growth.

This is topologically different from the MI distribution for the simplest NLSE, Hirota, and Sasa-Satsuma equations [16,20,23]. We expect that there could be some exotic dynamical excitations for this new MI distribution pattern. Moreover, the MS circle size can be changed by varying the strength of the fourth-order effect. When the semimajor axis is greater than $2A$, only a part of the ellipse is located in the MI band ($|\Omega| \leqslant 2A$). In this case, the MS regime which is located in the MI band is two curves. Moreover, when $\alpha = 0$, the MS circle decreases to become an MS point $(-\frac{\beta}{4\gamma}, 0)$ which is located on the resonance line in the MI band. Furthermore, for $\alpha < 0$, there is no MS regime in the MI band. To show the correspondence between MI and nonlinear excitations conveniently and clearly, we choose Fig. 1 (i.e., $\alpha > 2A$) to study the relation. Similar discussion can be made for other cases (i.e., $0 < \alpha < 2A$, $\alpha = 0$, and $\alpha < 0$), and we have proved that nonlinear excitations are the most abundant for the case in Fig. 1.

To obtain the correspondence relation between fundamental nonlinear waves and the MI distribution, we turn our attention to the exact solutions on the CWB. We derive an exact solution by means of the Darboux transformation method, which can describe many types of fundamental nonlinear excitations on a CWB. The explicit expressions for the solutions are presented in the Appendix. We can see that solution (A9) is a superposition of the CW and the perturbation signal ψ_s, which represents the nonlinear evolution process of the perturbation signal. Obviously, the form of solution (A9) and a linear superposition form of the CW and a perturbation signal in the linear stability analysis are consistent. Namely, the dynamic properties of these nonlinear waves can be understood by linear stability analysis. Furthermore, solution (A10) is a nonlinear combination of the trigonometric function ($\cos\varphi$) and hyperbolic function ($\cosh\phi$), where φ and ϕ are real functions of z and t [see Eq. (17)]. Here the hyperbolic function and trigonometric function describe the localization and the periodicity of the nonlinear waves, respectively. Hence the nonlinear wave described by solution (A10) can be seen as a nonlinear superposition of a soliton and a periodic wave. We find that solution (A10) contains eight types of fundamental nonlinear excitations: the Kuznetsov-Ma breather, nonrational W-shaped soliton ($\mathrm{WS_{nr}}$), antidark soliton, Akhmediev breather, periodic wave, W-shaped soliton train, rogue wave, and rational W-shaped soliton. The conditions for existence and the explicit expressions for these fundamental nonlinear excitations are listed in Table I.

MI is a process associated with the growth of perturbations on a CWB or other types of background. Here we mainly discuss the case of MI on a CWB. MI characters on a CWB are usually obtained by linear stability analysis with the linear superposition form $\psi_{\mathrm{signal}} + \psi_{\mathrm{cw}}$ (ψ_{signal} and ψ_{cw} denote the perturbation signal and the CWB, respectively). We note that localized waves on the CWB can also be written in a similar form. This provides the possibility of explaining the dynamics of the localized waves on the CWB through MI characters. Based on a Fourier analysis of the exact solutions of the rogue wave, Akhmediev breather, Kuznetsov-Ma breather, rational

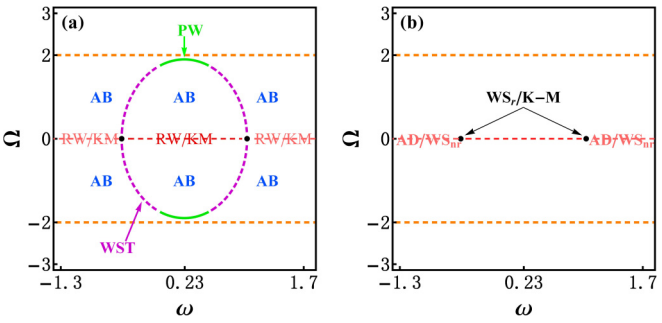

FIG. 2. (a) Phase diagram for different types of nonlinear waves on the modulation instability gain spectrum plane corresponding to Fig. 1. AB, Akhmediev breather; RW, rogue wave; K-M, Kuznetsov-Ma breather; PW, periodic wave; WST, W-shaped soliton train; WS$_r$, rational W-shaped soliton; AD, antidark soliton; WS$_{nr}$, W-shaped soliton. (b) Resonant line in the MI regime, on which AD and WS$_{nr}$ solitons can exist. Parameters are the same as in Fig. 1.

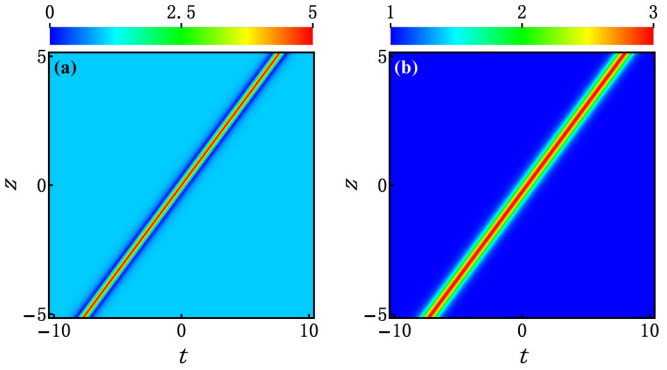

FIG. 3. Optical amplitude distributions $|\psi_s|$ of (a) a nonrational W-shaped soliton and (b) an antidark soliton on a continuous-wave background. Parameters are $A = 1, \beta = \frac{1}{12}, \gamma = -\frac{1}{36}, \omega = 0, b = 2$.

W-shaped soliton, nonrational W-shaped soliton, W-shaped soliton train, AD soliton, and periodic wave, we locate these different fundamental nonlinear excitations on the MI plane by defining and calculating the dominant frequency and propagation constant of each nonlinear wave [20], shown in Figs. 2(a) and 2(b). We can see that the rogue wave and Kuznetsov-Ma breather still come from the resonance perturbation in MI regimes and the Akhmediev breather still in the regime between the resonance line and the boundary line between the MI and the MS regime. These are similar to the rogue wave, Akhmediev breather, and Kuznetsov-Ma for the NLSE system. However, there are MS curves in the MI band for the fourth-order NLSE system and the periodic wave, W-shaped soliton train, and rational W-shaped soliton are excited in this regime [see Fig. 2(a)]. We have shown that the MS-regime structures in the MI regime depend on the parameter α [see Eq. (2)].

Therefore, stable nonlinear wave types are different for different α values. When the semimajor axis $\sqrt{6\alpha}$ of ellipse (2) is less than $\sqrt{3}A$ (i.e., $\alpha < \frac{A^2}{2}$), the periodic wave will not exist. Moreover, when $\alpha = 0$, the periodic wave and W-shaped soliton train do not exist. Furthermore, for $\alpha < 0$, stable nonlinear waves (periodic wave, W-shaped soliton train, and rational W-shaped soliton) do not exist in the MS regime in the MI band. We can see that several stable nonlinear waves exist only at two modulation stability curves; this condition seems to be very strict. However, in fact, with the background frequency and perturbation frequency approaching two modulation stability curves, the modulation instability gain G decreases rapidly, and the evolution distance of the rogue wave and Akhmediev breather increase rapidly and remain stable over a long propagation distance [30]. In this case, the dynamics of the rogue wave and Akhmediev breather behaves like that of the W-shaped soliton or periodic wave. In other words, although condition (2) of the modulation stability region is strict, these solitons and periodic waves still can be observed in experiments. The above results are consistent with those of previous investigations. The MI regime corresponds to unstable nonlinear waves (i.e., breathers and rogue waves) and the MS regime localized in the MI band corresponds to the excitations of stable nonlinear waves (i.e., solitons and periodic waves). However, we find that AD and WS$_{nr}$ solitons exist in the MI regime [see Fig. 2(b)], which seems to violate the prediction given by linear stability analysis. Particularly, they just exist in the MI regime outside the MS circle, and they cannot exist in the MI regime inside the MS circle. We discuss them in detail in the next section.

III. ANTIDARK SOLITONS AND W-SHAPED SOLITONS IN THE MI REGIME

The evolutions of AD and WS$_{nr}$ solitons are shown in Fig. 3; they indeed evolve with invariable profiles. It should be emphasized that MI characters can be used to explain the existence and evolution of localized waves on the CWB here. But the stability of these localized waves against perturbation cannot be explained by MI characters on the CWB. Their stability can be tested numerically by adding weak perturbations for their initial states or explained by performing MI analysis of all the localized wave solutions but not the CWB. Therefore, we test the stability of these solitons by adding some random noise to their initial states. As an example, we numerically test the stability of AD solitons against noise (initial condition $\psi_p = \psi_{AD}[1 + 0.01\,\text{random(t)}]$). The result is shown in Fig. 4(a), which indicates that the AD soliton is robust against noises. Furthermore, we perform direct numerical simulation of AD soliton by adding a weak Gaussian pulse perturbation, $\psi_{AD}[1 + 0.1e^{-(t+1)^2/4}]$, shown in Fig. 4(b). We can see that the AD soliton propagates stably, and a weak Gaussian pulse evolves into a rogue wave. After interacting with the rogue wave, the AD soliton is restored to its original shape by a small phase shift. This confirms that AD solitons indeed exist in the MI regime. This is significantly different from previous results showing that there is no stable localized wave in the MI regime [15,16,20,23]. The above analysis shows that AD and WS$_{nr}$ solitons exist under the same parameter condition $(\omega + \frac{\beta}{4\gamma})^2 - \frac{\delta^2}{6} = \alpha$ (where $\delta = 2\sqrt{b^2 - A^2}$). The structures of these two kinds of solitons are different [see Figs. 3(a) and 3(b)], but the energies of the AD and WS$_{nr}$ solitons against the CWB are identical, namely, $\varepsilon_{s1} = \varepsilon_{s2} = \varepsilon_s = 2\delta$. The perturbation energy ε of the pulse

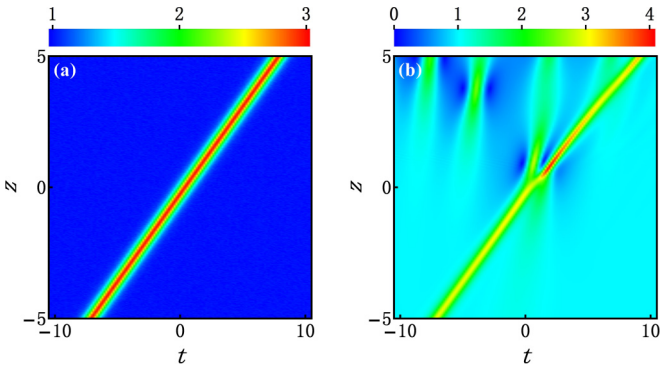

FIG. 4. (a) Numerical evolution from the initial conditions $\psi_p(t,-5)=\psi_{\rm AD}[1+0.01\,{\rm random}(t)]$. (b) Numerical evolution of $|\psi(t,z)|$ from the AD with the addition of weak Gaussian pulse perturbations in the form $\psi_{\rm AD}[1+0.1e^{-(t+1)^2/4}]$. Parameters are $A=1, \beta=\frac{1}{12}, \gamma=-\frac{1}{36}, \omega=0, b=2$.

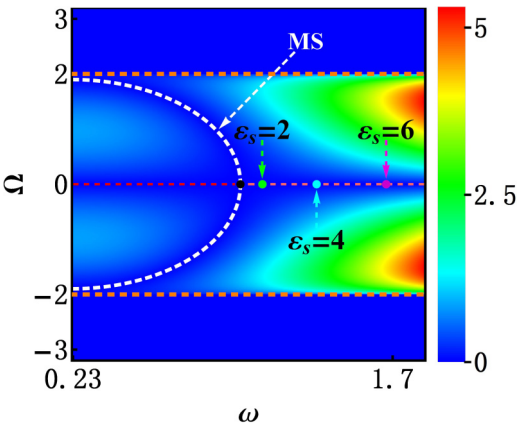

FIG. 5. Positions of the AD and WS_{nr} with different energies on the modulational instability gain spectrum plane. Green, aqua, and purple points correspond to the AD and WS_{nr} with different energies ε_s; blue points are modulation stability points on the resonance line. It shows that the position approaches the MS point as the perturbation energy decreases (the soliton amplitude becomes lower). Parameters are $A=1, \beta=\frac{1}{6}, \gamma=-\frac{5+\sqrt{15}}{48}$.

against the background is defined as

$$\varepsilon=\int_{-\infty}^{\infty}(|\psi|^2-A^2)dt. \tag{3}$$

Because there is a one-to-one correspondence between the parameter δ and the perturbation energy ε_s, we can rewrite the existence condition for AD and WS_{nr} solitons as follows:

$$\left(\omega+\frac{\beta}{4\gamma}\right)^2-\frac{\varepsilon_s^2}{24}=\alpha. \tag{4}$$

The condition has a clearer meaning since the perturbation energy has a clearer physical meaning than the parameter δ. Namely, for a specific system parameter and fixed background amplitude (i.e., β, γ, and A are fixed), when the background frequency ω and the energy of pulse ε_s satisfy Eq. (4), a CWB admits solitons with two special profiles (AD and WS_{nr} solitons) even in the MI regime (outside the MS circle). This character has not been found for the NLSE or its extended form with other types of high-order effects [9,15,16,24–30,42,43].

In order to better understand the generation mechanism of AD and WS_{nr} solitons, we analyze the relationship between their existence conditions and the MI gain. From the above linear stability analysis, the MS condition on the resonance line can be given as $\omega=-\frac{\beta}{4\gamma}\pm\sqrt{\alpha}$. This means that there are two MS points on the resonance line [see Fig. 2(a)]. Then we rewrite the existence conditions for AD and WS_{nr} solitons as follows:

$$\omega_s=-\frac{\beta}{4\gamma}\pm\sqrt{\frac{\varepsilon_s^2}{24}+\alpha}. \tag{5}$$

It suggest that AD and WS_{nr} solitons exist on both sides of two MS points on the resonance line [see Fig. 2(b)] (but do not exist in the regime between the two MS points). We plot the positions of AD and WS_{nr} solitons with different energies in Fig. 5. When the perturbation energy on a CWB corresponding to an AD or WS_{nr} soliton tends to 0 (the amplitude is low), stable soliton evolution agrees with the stability property predicted by linear stability analysis. But their excitation positions gradually deviate from the MS points as the energy increases. Namely, the energies of AD and WS_{nr} solitons are nonzero, and their excitation conditions do not agree with the MS condition predicted by linear stability analysis. Moreover, the other aforementioned localized waves with zero perturbation energies highly agree with the linear stability analysis; even the corresponding perturbation signals admit high amplitudes. These results indicate that linear analysis stability predictions agree with the evolution of strong perturbations with zero perturbation energy but do not agree with the evolution of strong perturbations with nonzero perturbation energy.

Therefore the perturbation energy also plays an important role in the evolution of perturbation signals. This means that a stable soliton with a high perturbation energy can exist in the MI regime predicted by linear stability analysis. This partly means that the perturbation energy could inhibit the MI properties. Considering that AD and WS_{nr} solitons can exist only with a specific perturbation energy on a certain CWB, we expect that there is a balance condition between perturbation energy and MI gain.

Thus, we would like to determine what factors create stable solitons in the MI regime. The above analysis indicates that the MI gain G and perturbation energy ε_s both play an important role in the excitation of the AD and WS_{nr} soliton. To further analyze the impact of the MI gain G and energy ε_s on the excitation of AD and WS_{nr} solitons, we simplify the expression of the gain G on the resonance line based on the above linear stability analysis result, $G=24A^2|\gamma||(\omega+\frac{\beta}{4\gamma})^2-\alpha|$. On the other hand, we can rewrite the energy squared expression for the AD and WS_{nr} solitons from Eq. (4), namely, $\varepsilon_s^2=24[(\omega+\frac{\beta}{4\gamma})^2-\alpha]$. The AD and WS_{nr} solitons do not exist when $(\omega+\frac{\beta}{4\gamma})^2-\alpha\leqslant 0$ [see the part between two MS points in Figs. 2(a) and 2(b)]. Therefore, we consider only the condition $(\omega+\frac{\beta}{4\gamma})^2-\alpha>0$. In this case, the MI gain G and the energy of the AD and WS_{nr} solitons satisfy

$$\frac{G}{\varepsilon_s^2}=A^2|\gamma|. \tag{6}$$

This can be seen as a balance condition between perturbation energy and MI. Obviously, fourth-order effects related to γ here cause the existence of AD and WS_{nr} solitons in the MI regime. This can be used to explain that AD and WS_{nr} solitons in the MI regime have not been found in the NLSE or its extended form with lower than fourth-order effects [9,16,23,26–30].

IV. DISCUSSION AND CONCLUSION

We present the correspondence relation between MI and fundamental excitations in the NLSE with both third-order and fourth-order effects. AD and WS_{nr} excitations are found to exist in the MI regime outside the MS circle (but not in the MI regime inside the MS circle), in sharp contrast to the correspondence relation for the simplest NLSE [20], Hirota equation [23], and Sasa-Satsuma equation [16]. We further test the evolutionary stability of solitons numerically, which indicates that they are robust against perturbations even in the MI regime. Solitons with high energies in the MI regime are caused by fourth-order effects. It is also meaningful to study excitation dynamics with other types of fourth-order or higher-order effects to determine whether there are some new MI properties. The results here further indicate that different MI distributions will bring different excitation patterns.

It has been well known that linear stability analysis holds well for weak perturbations. However, our results indicate that linear analysis stability predictions agree with the evolution of strong perturbations with zero perturbation energies but do not agree with the evolution of strong perturbations with nonzero perturbation energies. These characters are demonstrated by related exact soliton solutions on the CWB, but the underlying reasons for these striking characters are still unknown. Therefore, the development of some new ways to analyze the stability and dynamics of strong perturbations with nonzero perturbation energies is still needed.

ACKNOWLEDGMENTS

This work was supported by the National Natural Science Foundation of China (Contract No. 11475135) and a special research project of the Education Department of Shaanxi Provincial Government (Contract No. 16JK1763).

APPENDIX: THE GENERALIZED SOLUTION FOR FUNDAMENTAL NONLINEAR EXCITATIONS

The Lax pair of Eq. (1)is given as [36]

$$\Phi_t = U\Phi, \qquad \Phi_z = V\Phi, \tag{A1}$$

and

$$U = \begin{pmatrix} -i\lambda & \psi \\ -\psi^* & i\lambda \end{pmatrix}, \tag{A2}$$

$$V = \sum_{j=0}^{4} \lambda^j V_j, \tag{A3}$$

where

$$V_j = \begin{pmatrix} A_j & B_j \\ -B_j^* & -A_j \end{pmatrix}, \tag{A4}$$

$$\begin{aligned}
A_4 &= 8i\gamma, \quad B_4 = 0,\\
A_3 &= -4i\beta, \quad B_3 = -8\gamma\psi,\\
A_2 &= -i - 4i\gamma|\psi|^2, \quad B_2 = 4\beta\psi - 4i\gamma\psi_t,\\
A_1 &= 2i\beta|\psi|^2 - 2\gamma(\psi\psi_t^* - \psi_t\psi^*),\\
B_1 &= \psi + 4\gamma|\psi|^2\psi + 2i\beta\psi_t + 2\gamma\psi_{tt},\\
A_0 &= \tfrac{1}{2}i|\psi|^2 + 3i\gamma|\psi|^4 + \beta(\psi\psi_t^* - \psi_t\psi^*)\\
&\quad + i\gamma(\psi\psi_{tt}^* - |\psi|_t^2 + \psi_{tt}\psi^*),\\
B_0 &= -2\beta|\psi|^2\psi + \tfrac{1}{2}i\psi_t + 6i\gamma|\psi|^2\psi_t\\
&\quad - \beta\psi_{tt} + i\gamma\psi_{ttt}.
\end{aligned} \tag{A5}$$

The solution of Eq. (1) can be constructed as follows:

$$\psi = \psi_0 - 2i\frac{(\lambda - \lambda^*)\Phi_1\Phi_2^*}{|\Phi_1|^2 + |\Phi_2|^2}. \tag{A6}$$

In order to obtain nonlinear wave solutions on a plane-wave background, we first introduce the plane-wave solution $\psi_0 = Ae^{i(kz+\omega t)}$ of Eq. (1) as the seed solution of the Darboux transformation, where $\theta = \omega t + kz$ and $k = A^2 - \frac{1}{2}\omega + \beta(\omega^3 - 6A^2\omega) + \gamma(6A^4 - 12A^2\omega^2 + \omega^4)$. Substituting the plane-wave solution into Eq. (A1), we can obtain two sets of eigenfunctions,

$$\begin{pmatrix} \Phi_{11} \\ \Phi_{21} \end{pmatrix} = \begin{pmatrix} [i\lambda - \frac{1}{2}(\zeta - i\sigma) + \frac{i}{2}\omega]\phi_1 + A\phi_2 \\ A\phi_1 + [i\lambda - \frac{1}{2}(\zeta - i\sigma) + \frac{i}{2}\omega]\phi_2 \end{pmatrix} \tag{A7}$$

and

$$\begin{pmatrix} \Phi_{12} \\ \Phi_{22} \end{pmatrix} = \begin{bmatrix} A(\phi_1 + \phi_2) \\ (i\lambda + \frac{i}{2}\omega)(\phi_1 + \phi_2) + \frac{1}{2}((\zeta - i\sigma)(\phi_1 - \phi_2)) \end{bmatrix}, \tag{A8}$$

where $\phi_1 = e^{\tau_1 t + (C + B\tau_1 + i\tau_1^2)z}$, $\phi_2 = e^{\tau_2 t + (C + B\tau_2 + i\tau_2^2)z}$, $\lambda = -\frac{1}{2}\omega + ib (b > 0)$, $\zeta = (\sqrt{\chi^2} + \chi)^{1/2}/\sqrt{2}$, $\sigma = \pm(\sqrt{\chi^2} - \chi)^{1/2}/\sqrt{2}$, $\chi = 4b^2 - 4A^2$, $C = A^2 + \lambda^2 + \lambda\omega + \frac{1}{4}\omega$, $B = ib - \omega + \beta(-2A^2 - 4b^2 - 6ib\omega + 3\omega^2) + \gamma(4iA^2b + 8ib^3 - 8A^2\omega - 16b^2\omega - 12ib\omega^2 + 4\omega^3)$, and $\tau_1 = -\tau_2 = \frac{1}{2}\sqrt{-4A^2 - 4\lambda^2 - 4\lambda\omega - \omega^2}$.

Then the generalized exact solution of the NLSE with both third-order and fourth-order effects is derived to describe the types of fundamental nonlinear excitations. The solution is given as

$$\psi_{1,2} = Ae^{i\theta} + \psi_{s1,2}e^{i\theta}, \tag{A9}$$

where

$$\psi_{s1,2} = -A\frac{8b\Gamma_{1,2}(\cosh(\phi + \delta_{1,2}) + \cos(\varphi - \eta_{1,2}))}{\Delta_{1,2}\cosh(\phi + \tau_{1,2}) + \Xi_{1,2}\cos(\varphi - \rho_{1,2})}, \tag{A10}$$

with

$$\begin{aligned}
&\phi = \zeta t - V_1 z, \quad \varphi = \sigma t - V_2 z,\\
&V_1 = \zeta v_1 - b\sigma v_2, \quad V_2 = \sigma v_1 + b\zeta v_2,\\
&v_1 = \omega + \beta(2A^2 + 4b^2 - 3\omega^2) + 4\gamma(2A^2\omega + 4b^2\omega - \omega^3),\\
&v_2 = 1 - 6\beta\omega + 2\gamma(2A^2 + 4b^2 - 6\omega^2),\\
&\zeta = (\sqrt{\chi^2} + \chi)^{1/2}/\sqrt{2},\\
&\sigma = \pm(\sqrt{\chi^2} - \chi)^{1/2}/\sqrt{2},\\
&\chi = 4b^2 - 4A^2.
\end{aligned} \tag{A11}$$

The corresponding amplitude and phase notations are

$$\begin{aligned}
&\Gamma_1 = \sqrt{\beta_1^2 + \beta_2^2}, \quad \Gamma_2 = \sqrt{\alpha_1^2 - \alpha_2^2},\\
&\Delta_1 = 4A^2 + \beta_1^2 + \beta_2^2,\\
&\Delta_2 = \sqrt{(\alpha_3 + \alpha_4)^2 - 16b^2\zeta^2},\\
&\Xi_1 = -4A\beta_1,\\
&\Xi_2 = \sqrt{16b^2\sigma^2 + (\alpha_3 - \alpha_4)^2},
\end{aligned}$$

where $\cosh\delta_1 = \frac{\beta_1}{\Gamma_1}$, $\sinh\delta_1 = -\frac{\beta_2}{\Gamma_1}$, $\cosh\delta_2 = \frac{\alpha_1}{\Gamma_2}$, $\sinh\delta_2 = -\frac{\alpha_2}{\Gamma_2}$, $\cos\eta_1 = -\frac{4A^2+\beta_1^2+\beta_2^2}{4A\Gamma_1}$, $\sin\eta_1 = -i\frac{4A^2-\beta_1^2-\beta_2^2}{4A\Gamma_1}$, $\cos\eta_2 = \frac{\alpha_1}{\Gamma_2}$, $\sin\eta_2 = -i\frac{\alpha_2}{\Gamma_2}$, $\tau_1 = 0$, $\cosh\tau_2 = \frac{\alpha_3+\alpha_4}{\Delta_2}$, $\sinh\tau_2 = -\frac{4b\zeta}{\Delta_2}$, $\rho_1 = 0$, $\cos\rho_2 = \frac{\alpha_3-\alpha_4}{\Xi_2}$, $\sin\rho_2 = \frac{4b\sigma}{\Xi_2}$, $\alpha_1 = 2b$, $\alpha_2 = \zeta + i\sigma$, $\alpha_3 = 4A^2 + 4b^2$, $\alpha_4 = \zeta^2 + \sigma^2$, $\beta_1 = 2b + \zeta$, and $\beta_2 = \sigma$.

We find that solution (A10) contains eight types of fundamental nonlinear excitations: the Kuznetsov-Ma breather, nonrational W-shaped soliton, antidark soliton, Akhmediev breather, periodic wave, W-shaped soliton train, rogue wave, and rational W-shaped soliton train. The existence conditions and explicit expressions for these fundamental nonlinear excitations are listed in Table I.

[1] V. E. Zakharov and L. A. Ostrovsky, Physica D: Nonlin. Phenom. **238**, 540 (2009).
[2] N. Akhmediev and V. I. Korneev, Theor. Math. Phys. **69**, 1089 (1986).
[3] J. M. Dudley, G. Genty, F. Dias, B. Kibler, and N. Akhmediev, Opt. Express **17**, 21497 (2009).
[4] D. H. Peregrine, J. Aust. Math. Soc. Ser. B **25**, 16 (1983).
[5] B. Kibler, J. Fatome, C. Finot, G. Millot *et al.*, Nat. Phys. **6**, 790 (2010).
[6] E. A. Kuznetsov, Sov. Phys. Dokl. **22**, 507 (1977); Y. C. Ma, Stud. Appl. Math. **60**, 43 (1979).
[7] B. Kibler, J. Fatome, C. Fnot, G. Millot, G. Genty *et al.*, Sci. Rep. **2**, 463 (2012).
[8] B. L. Guo, L. M. Ling, and Q. P. Liu, Phys. Rev. E **85**, 026607 (2012).
[9] J. S. He, H. R. Zhang, L. H. Wang, K. Porsezian, and A. S. Fokas, Phys. Rev. E **87**, 052914 (2013).
[10] L. M. Ling, B. L. Guo, and L. C. Zhao, Phys. Rev. E **89**, 041201(R) (2014).
[11] A. Chabchoub and N. Akhmediev, Phys. Lett. A **377**, 2590 (2013).
[12] A. Chabchoub, N. Hoffmann, M. Onorato, A. Slunyaev, A. Sergeeva, E. Pelinovsky, and N. Akhmediev, Phys. Rev. E **86**, 056601 (2012).
[13] A. Chabchoub, N. Hoffmann, M. Onorato, and N. Akhmediev, Phys. Rev. X **2**, 011015 (2012).
[14] L. C. Zhao, G. G. Xin, and Z. Y. Yang, Phys. Rev. E **90**, 022918 (2014).
[15] L. C. Zhao, S. C. Li, and L. M. Ling, Phys. Rev. E **89**, 023210 (2014).
[16] L. C. Zhao, S. C. Li, and L. M. Ling, Phys. Rev. E **93**, 032215 (2016).
[17] F. Baronio, M. Conforti, A. Degasperis, S. Lombardo, M. Onorato, and S. Wabnitz, Phys. Rev. Lett. **113**, 034101 (2014).
[18] F. Baronio, S. Chen, P. Grelu, S. Wabnitz, and M. Conforti, Phys. Rev. A **91**, 033804 (2015).
[19] S. Chen, F. Baronio, J. M. Soto-Crespo, P. Grelu, M. Conforti, and S. Wabnitz, Phys. Rev. A **92**, 033847 (2015).
[20] L. C. Zhao and L. Ling, J. Opt. Soc. Am. B **33**, 850 (2016).
[21] S. Toenger, G. Genty, F. Dias, M. Erkintalo, and J. M. Dudley, Sci. Rep. **5**, 10380 (2015).
[22] M. Onorato, S. Residori, U. Bortolozzo, A. Montina, and F. T. Arecchi, Phys. Rep. **528**, 47 (2013).
[23] C. Liu, Z. Y. Yang, L. C. Zhao, L. Duan, G. Y. Yang, and W. L. Yang, Phys. Rev. E **94**, 042221 (2016).
[24] L. C. Zhao, Z. Y. Yang, and L. M. Ling, J. Phys. Soc. Jap. **83**, 104401 (2014).
[25] U. Bandelow and N. Akhmediev, Phys. Rev. E **86**, 026606 (2012); S. H. Chen, *ibid.* **88**, 023202 (2013).
[26] T. Xu, D. Wang, M. Li, and H. Liang, Phys. Scripta **89**, 075207 (2014).
[27] T. Xu, M. Li, and L. Li, Eur. Phys. Lett. **109**, 30006 (2015).
[28] A. Ankiewicz, J. M. Soto-Crespo, and N. Akhmediev, Phys. Rev. E **81**, 046602 (2010).
[29] Y. S. Tao and J. S. He, Phys. Rev. E **85**, 026601 (2012).
[30] C. Liu, Z. Y. Yang, L. C. Zhao, and W. L. Yang, Phys. Rev. E **91**, 022904 (2015).
[31] A. Blanco-Redondo, C. Martijn de Sterke, J. E. Sipe, T. F. Krauss, B. J. Eggleton, and C. Husko, Nat. Commun. **7**, 10427 (2016).
[32] M. Daniel and L. Kavitha, Phys. Rev. B **63**, 172302 (2001).
[33] M. Daniel, L. Kavitha, and R. Amuda, Phys. Rev. B **59**, 13774 (1999); M. Daniel and J. Beula, Chaos Solitons Fractals **41**, 1842 (2009).
[34] A. Ankiewicz, Y. Wang, S. Wabnitz, and N. Akhmediev, Phys. Rev. E **89**, 012907 (2014).
[35] L. Wang, J.-H. Zhang, Z.-Q. Wang, C. Liu, M. Lin, F.-H. Qi, and R. Guo, Phys. Rev. E **93**, 012214 (2016).
[36] A. Chowdury, D. J. Kedziora, A. Ankiewicz, and N. Akhmediev, Phys. Rev. E **90**, 032922 (2014).
[37] Y. Q. Yang, Z. Y. Yan, and B. A. Malomed, Chaos **25**, 103112 (2015).

[38] A. Chowdury, D. J. Kedziora, A. Ankiewicz, and N. Akhmediev, Phys. Rev. E **91**, 032928 (2015).
[39] A. Ankiewicz, D. J. Kedziora, A. Chowdury, U. Bandelow, and N. Akhmediev, Phys. Rev. E **93**, 012206 (2016).
[40] Y. Kodama, J. Stat. Phys. **39**, 597 (1985).
[41] G. P. Agrawal, J. Opt. Soc. Am. B **28**, A1 (2011).
[42] L. C. Zhao, C. Liu, and Z. Y. Yang, Commun. Nonlin. Sci. Numer. Simul. **20**, 9 (2015).
[43] X. Wang, B. Yang, Y. Chen, and Y. Q. Yang, Phys. Scripta **89**, 095210 (2014).